Research Article Vol. 32, No. 13 / 17 Jun 2024 / Optics Express 22817
Optics EXPRESS

Spatial distortions in swept source optical coherence tomography due to lateral scanning

ADRIAN FERNANDEZ UCEDA,* GOPIKA VENUGOPAL, AND ADRIAN PODOLEANU

Applied Optics Group, University of Kent, Giles Ln., Canterbury CT2 7NZ, United Kingdom
*af506@kent.ac.uk

Abstract: The paper presents errors in axial distance measurements and deviations of contours in swept source (SS) optical coherence tomography (OCT) cross sections due to lateral scanning. The study shows how these errors and deviations depend on the adjustments of the interface optics between a lateral scanner device and the target imaged. A theoretical model and experiments demonstrate that these errors and deviations are given by the Doppler shift frequency imprinted by the lateral scanning. The smaller the number of sweeps per lateral scanning interval, the larger these errors and deviations. The study also shows that the sign of error and deviation of contours can be put in correspondence with the spectral sweeping direction. Even more, it is shown that such effects can be used to predict the tuning direction of the swept source without an optical spectrum analyzer.

1. Introduction

The most modern OCT technology is based on processing of the optical spectrum at the interferometer output. In a spectrometer based OCT, this is done via a spectrometer and a broadband source [1,2]. In Swept Source (SS)-OCT, this is achieved via a balanced photodetector and a tunable laser (a swept source) [3] scanned across the sample.

The paper presents effects so far ignored in cross section SS-OCT images when performing lateral scanning. They affect the measurement of axial distances as well as the shapes of contours of the sample imaged, especially when the interface optics and the lateral scanner are not properly adjusted.

The importance of proper adjustment of the lateral scanner was identified early in the OCT evolution. Starting with time domain OCT, it was realized that optical path modulation due to lateral scanning can be used to generate *en-face* OCT images with no need of a phase or frequency modulator to create a carrier [4]. It was also known from the same imaging technology that offset position of the incident beam on the lateral scanner leads to optical path variation during scanning. This effect was already used in Newton rings imaging [5], enabling *en-face* OCT without an external phase modulator.

The off-pivot incidence of the beam on the line scanner was also employed in spectral domain OCT for elimination of the mirror terms [6], based on the associated Doppler effect introduced. Doppler frequency shifts due to movement of scattering centres was previously reported [7], however there was no anticipation of image distortion due to Doppler effects.

As consequence, the authors are not aware of any report on spatial errors in OCT along the axial direction due to lateral scanning. This study reports on such effects in a SS-OCT system. We show that incorrect adjustments of the interface optics, otherwise expected to affect lateral resolution performance, can also produce important effects in the axial direction in the A-scans and OCT cross section images (B-scans).

#520099 https://doi.org/10.1364/OE.520099
Journal © 2024 Received 25 Jan 2024; revised 26 May 2024; accepted 26 May 2024; published 6 Jun 2024

Optics EXPRESS

Let us consider a signal applied to the lateral scanner, where for a lateral deviation to address pixel m, the instantaneous voltage (for any shape of the signal, sinusoidal, sawtooth or triangular) is V_m. An axial deviation error (ADE) is introduced for each lateral pixel, m, in the B-scan OCT image, defined as the difference between the position in depth determined with the lateral scanner driven by the variable signal applied to the lateral scanner, and the position in depth determined with the lateral scanner at rest, but driven by a bias voltage = V_m.

The results obtained demonstrate that the ADE magnitude depends on the interface optics adjustments and on the number of sweeps within the lateral scanning interval. With reference to the interface optics, off-pivot errors or tilt of sample layers lead to ADE. The larger the amplitude of the lateral scanning, the larger the ADE. The ratio of the lateral scanning duration over the sweep duration gives the number of sweeps per lateral scanning interval. The larger the sweeping frequency in respect to the lateral scanning frequency, the smaller the ADE. For a given sweeping frequency, by increasing the frequency of lateral scanning, the number of sweeps per scanning interval reduces and ADE goes up.

For a given sweeping frequency and lateral scanning frequency, by enlarging the amplitude of the lateral scanning the ADE also goes up. This behavior suggests a dependence of the ADE on the scanning speed, proportional to the speed of variation of the optical path difference (OPD), that can be altered by either lateral scanning frequency or by its amplitude.

This report also demonstrates that the ADE sign depends on the direction of lateral scanning, as well as on the direction of spectral tuning. The ADE, if not minimized, can lead to distortions of images delivered and to errors in the axial position of sample structure. When the ADE magnitude is larger than the axial resolution interval, this prevents correct superposition of B-scans obtained with both lateral scanning directions, or correct superposition of images obtained using both tuning directions, in case of bidirectional tuning swept sources.

2. Theory

The ADE is evaluated experimentally for two cases of flying spot OCT imaging, employing two widely used interface optics in the sample arm of an OCT interferometer, for imaging skin and imaging retina, as shown in Fig. 1(s) and 1(e) respectively. Let us consider a mirror M as an object, and let us see how the B-scan of a mirror is affected by the adjustment of the interface optics in the system as well as by the direction of sweeping in the optical source. For simplicity, a single galvoscanner (GS) is shown.

In a first configuration considered, such as that in Fig. 1(s), a single lens, L1, of focal length, F1, is used at F1 from the GS pivot, P, with a mirror M placed behind the lens L1 at F1. Let us also consider that the mirror is tilted, obtained by rotation around a direction perpendicular to the sketch plane. At the extremity of lateral scanning, the sample ray travels plus or minus $\delta/2$ distance more than the ray to the point C, of intersection of the mirror with the optics axis, OZ.

In a second configuration, in Fig. 1(e), a system composed of 3 lenses is used, placing L1 at F1 from P, L2 is placed at $F1 + F2$ from L1, and L3 is placed at F2 from L2, being at the conjugate plane of the GS pivot, P. This is the preferred configuration for retina imaging, where the lens L3 plays the cumulative role of the cornea and eye lens of the eye under examination. In this configuration, the OPD variation shown by δ increases with deflection from on-axis, to either side of OZ. In Fig. 1(s), the OPD varies linearly with the deflection angle [4]. In Fig. 1(e), due to the curvature of the wavefront behind L3, the OPD varies quadratically with the deflection angle [5].

Let us consider the setup in Fig. 1(s) first. When laterally scanning the beam from one side to the other of the sample, for the case of a tilted mirror, M, the speed of OPD variation can be estimated via:

$$v = \frac{\delta}{T} \tag{1}$$

Optics EXPRESS

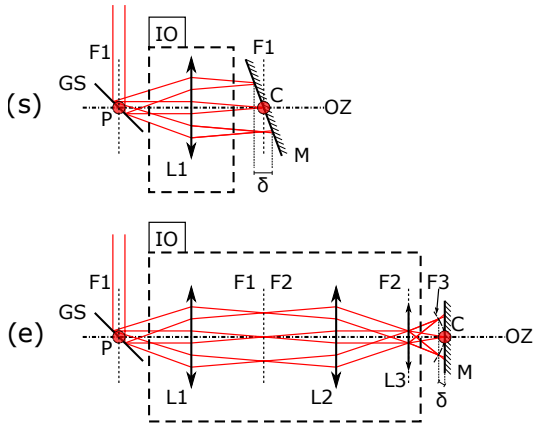

Fig. 1. Schematic diagrams of the interface optics (IO) used for imaging skin (s) and for imaging retina in an eye (e). GS: Galvanometer scanner; L1, L2, L3: lenses: L3: lens mimicking the focusing effect of the eye lens and cornea; F1, F2, F3: Focal distances corresponding to the lenses L1, L2 and L3; M: mirror; P: Pivot point of the GS; OZ: Optic axis; C: intersection of the axis OZ along depth and the mirror; δ: axial path variation encountered during lateral scanning.

where T is the duration of lateral scan from one edge of the scanned arc across the sample to the other edge. The arc scanned is the top of the B-scan, termed here as a 1D directional contour scanned, or a T-scan. A Doppler shift results, similar to the case of moving axially the reference mirror in the reference path, of frequency:

$$F = 2\frac{v}{\lambda} = 2\frac{\delta}{T \cdot \lambda} \tag{2}$$

The larger the tilt of the mirror, the larger δ, and the larger the Doppler frequency shift, F. The Doppler frequency shift combines with the frequency of the photodetected signal due to sweeping. For simplicity, let us consider linear variation of the optical frequency with the OPD (not affected by nonlinear sweeping or dispersion). For each increase of the OPD by an axial resolution interval, $2a$, the number of peaks in the channeled spectrum, N, increases by one (Eq. (22) in [8]). Hence, the number of peaks and troughs in the photodetected signal of the channeled spectrum can be written as:

$$N = \frac{OPD}{2a} \tag{3}$$

For N peaks read in the tuning interval τ, the frequency generated by sweeping is:

$$f = \frac{N}{\tau} \tag{4}$$

For a Gaussian spectrum shape of FWHM $\Delta\lambda$ in wavelength [9], the axial resolution in depth, a, is given by:

$$a = \frac{2\ln 2}{\pi}\frac{\lambda^2}{\Delta\lambda} \sim 0.44\frac{\lambda^2}{\Delta\lambda} \tag{5a}$$

However, the majority of swept sources exhibit a top hat spectrum shape, in which case the axial resolution interval is given by [10]

$$a \sim 0.6\frac{\lambda^2}{\Delta\lambda} \tag{5b}$$

Optics EXPRESS

The number of sweeps during the lateral scanning interval T is:

$$M = \frac{T}{\tau} \tag{6}$$

An axial deviation error, ADE, appears in the axial display of the T-scan of a mirror in the B-scan when the extreme point of the lateral angle is at a position along Z exceeding the correct position by more than an axial resolution interval:

$$ADE > a \tag{7}$$

This can happen when the Doppler frequency shift due to lateral scanning exceeds the frequency step $1/\tau$ in the spectrum of the photodetected channeled spectrum. For each added axial resolution interval to the OPD, the number of peaks in the channeled spectrum goes up by 1 and the frequency f goes up by $1/\tau$, hence using (2):

$$2\frac{\delta}{T \cdot \lambda} > \frac{1}{\tau} \tag{8}$$

Then using (6):

$$\frac{\delta}{M} > \frac{\lambda}{2} \tag{9}$$

In other words, when half of the OPD variation encountered by lateral scanning over a transversal pixel size exceeds half of a wavelength, it is expected that ADE becomes visible.

For good imaging, the number of sweeps in a T-scan, M should exceed several hundreds, however when M becomes so small that (9) is satisfied, errors become visible in the B-scan OCT image.

2.1. Phase variation

Let us consider the interface optics in Fig. 1 as part of the sample arm of an OCT interferometer. Due to lateral scanning with a velocity, v, the sample path length, L_S varies in time over an initial value L_{S0} according to:

$$L_s = L_{s0} + vt \tag{10}$$

The reference path length L_R in the OCT interferometer can be written respectively as:

$$L_R = L_{R0} \tag{11}$$

where L_{R0} is an initial length kept constant. When the sample beam is directed at $t = 0$ to the top edge of the object in Fig. 1(s), above the center of the image at C, half of the OPD can be written as:

$$L_{S0} - L_{R0} = z \tag{12}$$

whilst the OPD/2 with the beam deviated from the top edge due to lateral scanning is:

$$L_S - L_R = z + vt \tag{13}$$

At the extremes of lateral scanning, the axial deviation is $\delta/2$ or $-\delta/2$, separated in time from the moment when the scanning beam hits the point on axis, C, by half the period of the signal driving the galvoscanner GS, $T/2$. Considering the time t within a τ interval, while the scanning

Optics EXPRESS

beam is deflected over the pixel m (where m is between 1 and M), an expression can be obtained for the phase of the photodetected signal at the output of the OCT interferometer:

$$\varphi_m(t) = k(t)\left[z + (m-1)\frac{\delta}{M} + \frac{\delta t}{\tau M}\right] \tag{14}$$

where the wavenumber variation during each sweep of duration, τ, in time can be written as:

$$k(t) = K_1 + \frac{\Delta K}{\tau}t \tag{15}$$

Here K_1 is the initial wavenumber and K_2 is the final wavenumber after a tuning time interval τ

$$\Delta K = K_2 - K_1 \tag{16}$$

When tuning from a small wavelength, λ_1 to a large wavelength, λ_2, $\Delta K<0$ whilst when tuning from a large wavelength to a small wavelength, $\Delta K>0$. Using

$$\frac{\delta}{M\tau} = \frac{\delta}{T} = v \tag{17}$$

(14) becomes:

$$\varphi_m(t) = k(t)\left[z + (m-1)\frac{\delta}{M} + vt\right] \tag{18}$$

Introducing (15) into (14) and performing a time derivative, the instantaneous frequency of the photodetected signal is obtained as:

$$\frac{d\varphi_m}{dt} = \frac{\Delta K}{\tau}\left[z + (m-1)\frac{\delta}{M} + vt\right] + k(t)v \tag{19}$$

In the middle of a sweeping interval τ corresponding to lateral scanning over the lateral pixel m, i.e., for:

$$t = \frac{\tau}{2} \tag{20}$$

(19) becomes:

$$\omega_m = \frac{\Delta K}{\tau}\left[z + (m-1)\frac{\delta}{M} + v\frac{\tau}{2}\right] + k\left(\frac{\tau}{2}\right)v \tag{21}$$

Given the fact that:

$$k\left(\frac{\tau}{2}\right) = K_1 + \frac{\Delta K}{2} = \frac{K_2 + K_1}{2} = K_c \tag{22}$$

where K_c is the central wavenumber, (19) becomes:

$$\omega_m = \frac{\Delta K}{\tau}\left[z + (m-1)\frac{\delta}{M} + v\frac{\tau}{2}\right] + K_c v \tag{23}$$

The first term determines the frequency of the photodetected signal due to the sweeping, proportional to the OPD, i.e., due to the modulation of the spectrum into a channeled shape,

Optics EXPRESS

hence denoted as ω_{CS}:

$$\omega_{cs} = \frac{\Delta K}{\tau}\left[z + (m-1)\frac{\delta}{M} + v\frac{\tau}{2}\right] \tag{24}$$

As

$$v\frac{\tau}{2} = \frac{\delta}{2M} \ll \delta \text{ and } \delta \ll z \tag{25a, 25b}$$

$$\omega_{cs} \sim \frac{\Delta K}{\tau} z \tag{26}$$

The last term in (23) can be put under the form:

$$\omega_D = vK_c = 2\pi F_D \tag{27}$$

and represents the Doppler shift. This shows that the Doppler shift is proportional to the velocity of varying the OPD, as expected. This depends on the amplitude and frequency of the driving signal applied to the GS.

If the beam would be stationary on C, ω_{CS} would be the only frequency term and the tilt of the mirror would be correctly displayed by the B-scan. Due to lateral scanning, the frequency of the photodetected signal varies from ω_{CS} by ω_D.

2.2. *Predicting the profile of Doppler shift variation during lateral scanning*

Let us consider the signal driving the GS as triangular, of period 2T, as illustrated in the top row of the table in Fig. 2. Let us also consider that the target is a mirror, that in the case of (s) configuration is tilted. For the sake of illustration, an exaggerated tilt of 45 degrees was considered and the variation of optical path, δ, calculated in the table in Fig. 2, middle row left. In configuration (e), the mirror was considered oriented normally to the optical axis. The path variation is quadratic in this case, hence δ will vary along a parabola. δ is considered zero at the beginning of the lateral scan for both (s) and (e) configurations. In the middle of the lateral scan, for 0.5T, when the scanning beam reaches point C (Fig. 1) in (s) $\delta = 0.5$ while in (e) is maximum, 1 (considered as a normalized value to maximum deviation). At the end of the lateral scan, at time equal to 1, i.e., for T, in (s) deviation δ is maximum, i.e., 1 while in (e) deviation returned to zero.

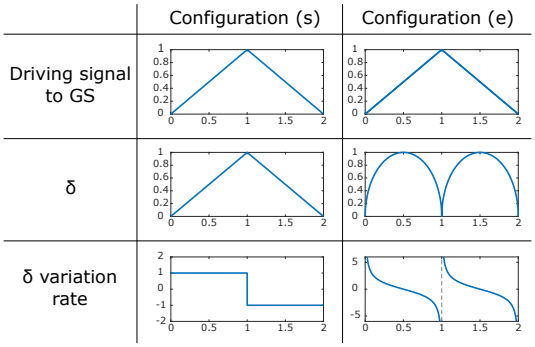

Fig. 2. Approximate illustration of the δ and its variation rate for each configuration in Fig. 1 versus time during lateral scanning. Doppler frequency shifts due to variation of δ in the middle row are shown in the bottom row.

The time on the horizontal axis in all illustrative graphs in Fig. 2 is in units of T, where T is the half period of the triangular signal applied to the GS. What determines the Doppler shift is the variation rate of δ, illustrated in the third row. In configuration (s), the variation rate is expected

Optics EXPRESS

to be constant, which will lead to a constant ADE across the B-scan. This ADE will change signs depending on the scanning direction. In configuration (e), due to the parabolic shape of δ, the ADE will be larger at the edges than at the center of the B-scan, and the sign will remain the same regardless of the scanning direction. The resulting B-scans for a mirror will be distorted, following the profile obtained by adding the contours in the middle and bottom rows in Fig. 2

3. Experimental setup

The schematic diagram of the OCT setup is shown in Fig. 3. This consists in an interferometer based on a beamsplitter, BS, and a 50/50 fiber coupler, FC, terminated on a balanced photodetector, BPD. The photodetected signal delivered by the BPD is sampled by an ATS 9350 AlazarTech card digitizer placed in a computer. A lateral 2D scanning head scans the beam over the sample via an interface optics, IO, such as shown in Fig. 1. The 2D scanning head is composed of two orthogonally placed galvanometer scanners, (not shown), determining the line in the raster and the frame rate. The theory presented above refers to the galvanometer scanner determining the line, labeled in continuation as GS, that is driven faster than the frame galvanometer scanner. Depending the case, the role of GS was played by one or the other galvanometer scanner in the scanning head.

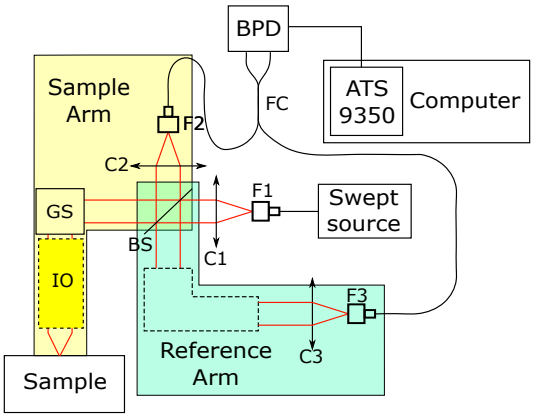

Fig. 3. Schematic diagram of the OCT setup employed. IO: interface optics; F1-3: fiber mounts; C1-3: collimator; BS: Beamsplitter; FC: 50/50 fiber coupler; GS: Galvanometer scanner; BPD: Balanced photodetector.

To fully evaluate the conditions that lead to ADE, the GS was driven with triangular signals at different amplitudes and frequency and for most data collections here the frame galvoscanner was set at rest. The interface optics (IO) discussed in Fig. 1 were evaluated under the excitation of three swept sources (SS). (i) CSU-SS, a commercial slow unidirectional tuning SS, Broadsweeper BS-840-2 (Superlum) with a sweep rate of 2 kHz. The spectral emission is centered at 850 nm, starting at 872 nm and finishing the sweep at 828 nm; (ii) RSB-SS, an own assembled bidirectional SS using a resonant scanner driven at $1/(2\tau) = 16$ kHz [11], sweeping between 850.5 nm and 859.5 nm, equivalent to tuning at a frequency of 32 kHz during each half period, τ; (iii) CFU-SS, a commercial fast unidirectional tuning SS, Axsun sweeping at 100 kHz, central wavelength 1060 nm

The CSU-SS exhibits a top hat spectrum, in which case applying (5b) for a bandwidth $\Delta\lambda = 44$ nm, $a \sim 10$ µm. The RSB-SS exhibits a Gaussian spectrum, hence using (5a) and $\Delta\lambda \simeq 9.5$ nm gives $a \sim 33$ µm. The CFU-SS exhibits a $\Delta\lambda = 100$ nm according to its data sheet, that should have a top hat spectrum, resulting in $a \sim 6$ µm using (5b), however, its spectrum is a combination

Optics EXPRESS

of two Gaussian peaks, resulting on a reduced axial resolution of $a \sim 9$ μm. The axial resolution measured of the three SSs were respectively: $a \sim 10$, 33 and 9 μm.

The resonant scanner driver of the RSB-SS delivers a TTL trigger to synchronize external instruments, with two sweeps per trigger. This can be conveniently delayed in relation to the sinusoidal signal applied to the resonant scanner by actuating on a front panel potentiometer. Figure 4 presents 3 traces. The TTL signal shown in yellow on the top trace is the trigger sent to the digitizer. In red, middle trace represents the sinusoidal signal sent to the resonant mirror used for the sweeping in the RSB-SS. The bottom trace in yellow shows the photodetector signal at the interferometer output. This presents a channeled aspect, where the larger the optical path difference in the interferometer, the denser its modulation [12].

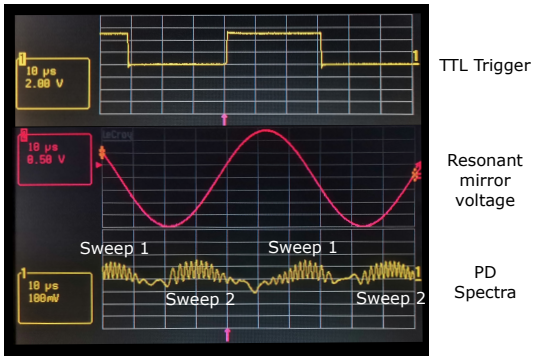

Fig. 4. Channeled spectrum (bottom trace, yellow) versus the sinusoidal signal applied to the resonant scanner (middle trace, red) in the RSB-SS and the trigger signal (top trace, yellow). The GSs were kept at rest.

Because electrical cables used to convey the three signals to the scope are of different lengths, the transitions on the trigger signal are slightly displaced laterally in respect to the other two waveforms in Fig. 4. In LabView, trigger is delayed digitally in order to shift the fly-back outside of the displayed image.

One sweep falls under the 5 V part of the trigger, while the second sweep falls under the 0 V part of the trigger. The spectrum is split in half and the sweep under 5 V is denoted as "Sweep 1" whilst the sweep under 0 V is denoted as "Sweep 2". Later below these sweeps will be put in correspondence with the backwards and forward sweeping performed by the RSB-SS.

4. Experimental results

The estimated behavior for δ and its variation presented in Fig. 2 can be confirmed by performing *en-face* TD-OCT in both configurations and observing the pattern formed in the image due to the interface optics. These patterns can be seen in Fig. 5. The images were obtained with the CSU-SS source emitting a narrow spectral emission (non sweeping) and driving both galvanometer scanners, obtaining a 2D *en-face* time domain OCT image. In configuration (s), a regular pattern of parallel lines are obtained [4]. The tilt of lines is due to the mirror surface being inclined in respect to both X and Y axes. In configuration (e), Newton rings [5] appear, where the distance between adjacent rings decreases for rings further away from the center. Some artefacts can be observed at the edges of both images. In the case of configuration (s), these artefacts are due to the acceleration of the galvoscanners, while in the configuration (e), the artefacts are due to aliasing effects.

Optics EXPRESS

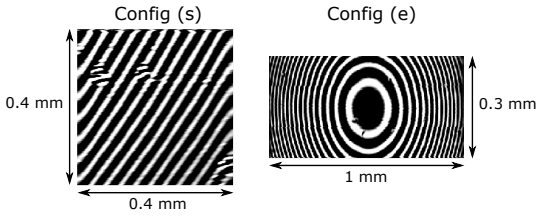

Fig. 5. *En-face* TD-OCT image obtained from a flat mirror using configurations (s) and (e). In the configuration (s) the size scanned horizontally is similar to that scanned vertically, of 0.4 mm, corresponding to an amplitude of 0.1 V applied to both galvanometer scanners. The frequency of the triangle signal applied to the galvanometer scanner (line) for scanning horizontally was 500 Hz (T = 1 ms) while the frequency of the signal driving the galvanometer scanner for scanning vertically (frame) was set to 1 Hz (i.e., leading to a C-scan made from 500 T-scans). In the configuration (e), the voltages applied to the two galvanometer scanners were1 V and 0.2 V respectively, and the image was cropped to show the central rings. The frequency of the triangle signal driving the line galvanometer scanner was 80 Hz (T = 6.25 ms) and that of the signal driving the frame galvanometer scanner was 0.4 Hz.

4.1. Configuration (s)

4.1.1. SS-OCT where the swept source performs unidirectional sweeping

In order to evaluate the distortions affecting the B-scan OCT images based on the SS-OCT method, three different measurements in each configuration are performed using the CSU-SS: the first measurement consists of a 1D TD-OCT image obtained by driving the line galvanometer scanner only, in contrast to the 2D TD-OCT image from Fig. 5, in order to isolate the distortions in a single scanning axis only; the second measurement is obtained from an electrical Spectrum Analyzer that measures the RF spectrum of the photodetected signal; the third measurement consists of a B-scan obtained with the full tuning bandwidth of the CSU-SS. In the first two measurements, the line galvanometer scanner, playing the role of GS in Fig. 1, was driven at the same rate of 80 Hz, while in the 3rd set at both 80 Hz and 160 Hz as detailed further below. These results are presented in Fig. 6 for the configuration (s) and later on, in Fig. 9 for configuration (e).

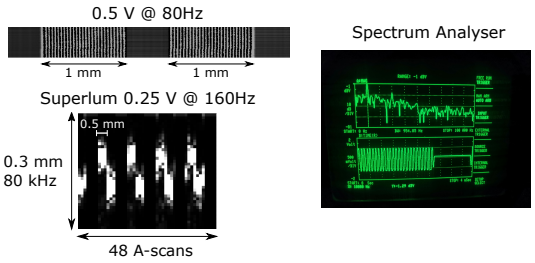

Fig. 6. Three procedures to evaluate the ADE in configuration (s) using the CSU-SS. Only the line galvanometer scanner, playing the role of GS in Fig. 1, is driven, while the other galvanometer scanner is at rest. Top left: TD *en-face* fringe pattern from a mirror behind a 1 mm slit with CSU-SS non sweeping; Right: frequency spectrum at the top and temporal evolution at the bottom of the photodetected signal in TD *en-face* OCT with non sweeping CSU-SS (the spectrum analyzer display corresponds to both cases of either 0.5 V at 80 Hz or 0.25 V at 160 Hz); Bottom left: cross section (B-scan) image obtained by sweeping the CSU-SS.

From the TD-OCT image presented in Fig. 6, a prediction of the ADE value expected in SS-OCT can be made. With a slit size of 1 mm, which is a 43% of the image size, the number of

Optics EXPRESS

fringes is reduced by a factor of 0.43. 27 fringes are seen in the image in Fig. 6 top left. This means that within a lateral scan, there are ~ 63 fringes. The number of fringes corresponds to a path variation $\delta = 63\lambda/2 = 27$ μm. For $2T$ = [parse-numbers=false]1/80 Hz, this leads to a speed of z variation of $v = \delta/T = 4.3$ mm/s. Then a Doppler shift = $F = 2v/\lambda \sim 10$ kHz can be evaluated. As this is larger than the sweeping frequency of 2 kHz, an ADE is expected according to (8).

Indeed, the spectrum analyzer in Fig. 6 right shows the main component at 10 kHz. In the SS-OCT B-scan image in Fig. 6 bottom left, a peak to peak depth variation of 20 kHz is measured. This is because each ramp of the GS leads to ADEs of opposite signs, so the frequency shift corresponding to ADE during each GS ramp is 10 kHz. The agreement of the two ADE values obtained by using either procedure in Fig. 6 suggests that in practice either TD or SS-OCT method can be used to evaluate the number of fringes per lateral scan, and consequently, the correct adjustment of the interface optics (tilt of mirror and hence δ).

For each increase of OPD by an axial resolution interval ($a = 10$ μm), according to Eq. (5b), the frequency of the read signal increases by the sweeping frequency, i.e., by 2 kHz. Therefore, for any of the 3 methods above, the ADE can be ignored if the Doppler shift is less than the frequency pixel of 2 kHz. This determines a maximum speed of $(\lambda/2)\cdot 2$ kHz = 0.85 mm/s, when speed exceeds this values, then distortion takes place. For the case in Fig. 6, speed is 4.3 mm/s, i.e., larger, so an ADE is expected. Obviously, a Doppler shift of 10 kHz exceeds by a factor of 5 the frequency pixel of 2 kHz. This factor is similar to that obtained by the ratio of the current speed of 4.3 mm/s over the maximum speed value evaluated above of 0.85 mm/s.

4.1.2. SS-OCT where the swept source performs bidirectional sweeping

Swapping the CSU-SS with the RSB-SS presents a new effect, as portrayed in Fig. 7(a). Since the RSB-SS performs bidirectional sweeping, as presented in Fig. 4, to generate a B-scan, the A-scans due to each sweep need to be intercalated. Therefore, if the A-scans from Sweep 1 are labeled as S11, S12, S13, . . . S1n and the A-scans from Sweep 2 are named as S21, S22, S23, . . . S2n, a B-scan obtained with the RSB-SS will be composed of A-scans S11, S21, S12, S22, . . . S1n, S2n.

Whilst previously with the CSU-SS the ADE was constant over the half period of lateral scanning T, now in Fig. 7(a), with the RSB-SS, the ADE changes sign between each A-scan, causing breaks in the B-scan. If the A-scans are separated according to their sweeping direction, as shown in Fig. 7(b), the Sweep 1 experiences an opposite ADE in respect to the ADE of Sweep 2.

When obtaining data from the RSB-SS, we recorded every other trigger and used the time of the second trigger to split and construct the A-scans. This means that for each pair of sweeps, that were obtained, sweep 1 and sweep 2 (as labeled in Fig. 4), the next pair was not recorded. This means that for example, if the recording time is set to 1 ms, given $2\tau = 1/(16$ kHz), we retain and record 8 pairs of A-scans, instead of 16.

To obtain Fig. 7, only the line galvanometer scanner, GS, is driven. A triangular signal was applied to GS of 1 V amplitude and $1/(2T) = 666$ Hz, scanning laterally ~ 4 mm of a flat mirror as a sample for each half period $T = 0.75$ ms. For the B-scan display, both ramps are recorded 4 times, obtaining a total of 8 B-scans in 6 ms. During each period 2T of the GS signal, there are M = 12 A-scans, summing up to 48 A-scans for each sweeping direction. Due to bidirectional sweeping of the RSB-SS, there are 96 A-scans in the display of the 8 B-scans. Considering the size of the B-scan along axis Z of 960 μm, the top of the B-scans corresponding to the two sweep direction are axially shifted in respect to each other by 192 kHz. This corresponds to an ADE for each sweep of 96 kHz, i.e., of ~ 3 axial frequency pixels (determined by the resonant scanner half period of 1/32 kHz). Clearly, such high ADE level prevents generating a correct B-scan, with a single, contiguous well defined image contour.

Optics EXPRESS

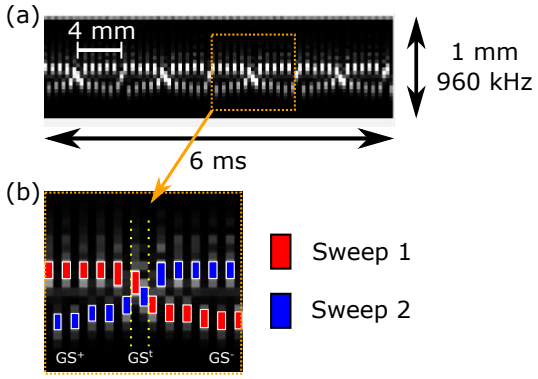

Fig. 7. B-scans from a mirror obtained using SS-OCT employing the RSB-SS: (a) The image contains 4 full periods of the GS driven at 666.67 Hz and 1 V amplitude, creating a total of 8 B-scans per image of 4 mm lateral size of the mirror (extending for 6 ms). Vertical axis represents 960 kHz (~ 1 mm). (b): a zoomed section of the third period is presented. The A-scans corresponding to Sweep 1 are shown in red, while the A-scans from Sweep 2 are shown in blue. The positive slope of the GS is marked as GS^{+}, its negative slope as GS^{-}, and the transition between both slopes is marked as GS^{t}. In the mid of the transition, the speed of the GS approaches 0 and the ADE disappears. As the GS accelerates, the ADE increases again.

To understand the nature of the ADE, several experiments were performed by changing the different parameters at which the GS is moved, with B-scans obtained as shown in Fig. 8, and measuring the axial separation between consecutive B-scans, each obtained from a different slope of the GS. First, the GS was run at 166 Hz where a small variation on OPD was noticed, giving an error in axial positioning between contours of 32 kHz (33 μm) in the first column. When doubling the amplitude of the driving signal from 0.5 V to 1 V, the amplitude of the ADE doubled. Then by doubling the frequency to 333 Hz while reducing to 0.5 V amplitude the same ADE value was obtained.

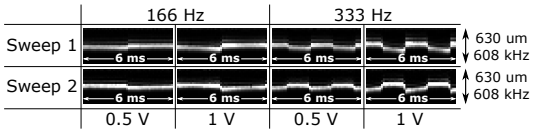

Fig. 8. Comparison of B-scans obtained using SS-OCT employing the RSB-SS, for two values of voltage and frequency of the signal applied to the GS. The vertical size in all B-scans is 630 μm along the axial coordinate Z, corresponding in frequency to 608 kHz.

A slip between contours value of 64 kHz (66 μm), corresponding to an ADE of 32 kHz (33 μm), at 166 Hz and 1 V is similar to that obtained for 166 Hz and 0.5 V, presented in both the 2nd and 3rd column respectively. This implies that the ADE is directly proportional to the angular speed of the GS, that can be modified either by frequency or amplitude of the signal applied. Obviously such a behavior can be attributed to the Doppler shift coming from the lateral scanning imprinted by the GS in the system, which depends on both the amplitude and frequency of the lateral scanning when the target is a tilted mirror. In the last column, with a frequency of 333 Hz and an amplitude of 1 V, the distance between contours is ~ 128 kHz (132 μm).

In the 1st column in Fig. 8, the ADE is almost equal to half of the axial resolution interval of a = 33 μm. For each advance in z by a, the electrical signal spectrum advances by a frequency

Optics EXPRESS

pixel interval of $1/\tau$ = 32 kHz. In the 2nd an 3rd column, the distance between contours is ~ 2 frequency pixels = 2 axial resolution pixels, $2a$, while in the 4th column it is ~ $4a$. This correlates with an ADE for each ramp of the GS of $1a$ and $2a$ respectively. The acquisition time for each B-scan is 6 ms. The 166 Hz group covers the full period 2T of the driving signal, while the 333 Hz group covers two periods, i.e., 4T. Each image is comprised of 48 A-scans, having 24 A-scans per half period T when $1/(2T)$ = 166 Hz and 12 A-scans per half period T at 333 Hz. At 0.5 V, the scanned lateral size over the mirror was 2 mm, while at 1 V it was 4 mm, as in Fig. 6.

The larger the velocity of lateral scanning, the larger the frequency deviation of the frequency spectrum read by the photodetector during a sweeping time interval, τ. In the case of the interface optics in Fig. 1(s), a tilt of the mirror leads to a Doppler shift that is constant during each lateral deflecting interval T. Obviously, during the next deflecting interval T, the direction of OPD variation changes, meaning that the frequency spectrum of the electrical signal (read at the photodetector output by sweeping through the spectrum) will suffer deviations in opposite directions during the two lateral scanning intervals T given by half period of lateral scanning, of period 2T, as illustrated in Fig. 4. The shapes of B-scans in Fig. 6, 7 and 8 are in line with the expectations predicted by the bottom row in Fig. 2 left.

4.2. Configuration (e)

4.2.1. SS-OCT where the swept source performs unidirectional sweeping

In the examples above, the velocity in OPD variation is constant during the lateral scanning half period, T. This is also proven by the uniform separation of the fringes in the TD OCT image in Fig. 6.

For the case of imaging the eye, as shown in Fig. 2(e), the velocity varies nonlinearly, as presented in [5]. As the OPD varies via a square law in relation to the angle of scanning [5,13], during each lateral scanning interval T, the velocity is either positive or negative, going through zero on axis (if the incident beam is exactly on the GS pivot).

As in Fig. 6 for configuration (s), we started by comparing TD-OCT, B-scans and the electrical spectrum analyzer signal. These results are presented in Fig. 9. The source employed for all the sets was the CSU-SS. This time, since we expect the ADE to not be constant (according to Fig. 2 right bottom), we also compared results for two different GS speed rates. First row corresponds to 0.5 V amplitude and 80 Hz frequency, same as in Fig. 6, and the second row corresponds to doubling the lateral scanning speed by applying double of amplitude, 1 V at 80 Hz. The mirror object scanned was set behind a slit of 1 mm width as in Fig. 6.

This time, both TD-OCT and the spectrum analyzer procedure display a chirp in periodicity. This makes the exact calculation of ADE dependent on the position of the pixel in the T-scan. The B-scans in the 3rd column in Fig. 9 show a tilt in agreement with the predictions in Fig. 2 bottom row right.

To study the relationship between the tilt of contours in Fig. 9(c) column, and the speed of the scanner, we repeated similar measurements as performed for the configuration in Fig. 1(s).

Using the CSU-SS, we obtained Fig. 10, in which 2.5 periods of the driving signal are shown, i.e., 2.5 B-scans. Within each half period, for small voltages, the profile in Fig. 2 bottom left is visible, similar to that in configuration (s), i.e., from one half period to next, the T-scans jumps axially. This may be due to a small tilt of the mirror, in which case, when the amplitude is small, all lateral scan is within one side of point C in Fig. 1. At larger amplitudes, the lateral scan crosses the other side of point C and the offset is less visible.

Number M of A-scans in each half period T = 6.25 ms is M = 2 kHz/160 Hz = 12 A-scans. At 0.25 V, when M is larger than 12, ADE can be ignored. Otherwise, more than M = 48 A-scans are needed at 1 V to ignore the ADE, requiring a reduction of the lateral scan rate to less than 20 Hz.

Optics EXPRESS

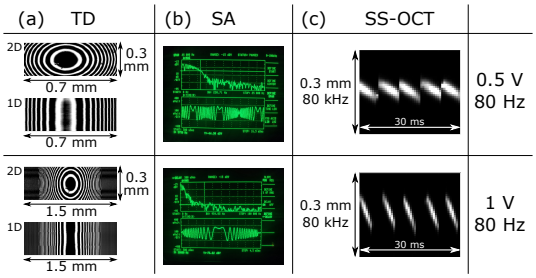

Fig. 9. Three procedures to evaluate the ADE in configuration (e) using the CSU-SS. (a): 2D and 1D TD *en-face* fringe pattern from a mirror behind a 1 mm slit with CSU-SS non sweeping, top with both galvanometer scanners driven, bottom using the line galvanometer scanner only, acting as GS from Fig. 1; (b): frequency spectrum at the top and temporal evolution at the bottom of the photodetected signal in TD *en-face* OCT with CSU-SS non sweeping; (c): cross section (B-scan) images using SS-OCT. First row corresponds to driving the GS at 80 Hz with 0.5 V amplitude, while in the second row the GS was driven at 80 Hz with 1 V amplitude.

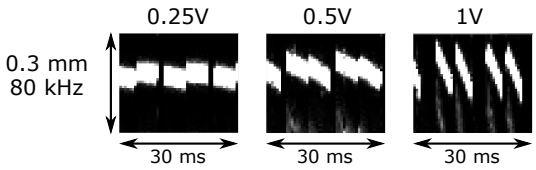

Fig. 10. Comparison of B-scans of a flat mirror covered with a slit using the CSU-SS in configuration (e). The frequency of the signal used for lateral scanning was kept constant at 80 Hz, while the amplitude of scanning was increased in double steps.

4.2.2. SS-OCT where the swept source performs bidirectional sweeping

Using the RSB-SS, Fig. 11, is obtained, where the tilts of the T-scans are shown. The higher the voltage, and the higher the scanning frequency of the triangular signal applied to GS, the larger the tilt. The contours displayed are, to some extent, similar in shape with the profiles predicted in the right sketch of the bottom row in Fig. 2. As they extend over a few pixels in depth only, they cannot follow the exact shape predicted. However, for each half period T, the tilt is evident. At 160 Hz frequency (corresponding on each ramp to 320 Hz) and 1 V amplitude, the ADE is 250 μm, ~ 240 kHz. A conversion C = 1.04 μm/kHz relates the frequency deviation to the ADE. In the RF spectrum of the photodetected signal, pixels are separated by $1/\tau$ = 32 kHz and along depth by 33.28 μm. A variation in frequency of 240 kHz means an ADE of 240/32 = 7.5 axial resolution pixels, of size a each, along the depth coordinate, z.

In Fig. 11(a), there are M = 16/0.32 = 50 A-scans per each ramp in either sweeping direction. ADE is barely perceptible. This means that for M > 50, the error can be ignored. However if the amplitude of scanning is increased, as shown in (b), the number of A-scans, M, should be increased accordingly (for instance by at least doubling the sweeping speed, if that would be possible) in order to maintain the ADE below the axial resolution interval, a, where it could be ignored. In order to compare the tilts experienced with both sources, Fig. 12 presents tilts of T-scans in the B-scans obtained for a GS driving signal of different scanning frequency with the RSB-SS (a) and the CSU-SS (b) against the T-scan obtained with the sample beam stationary. The larger the scanning speed, the larger the tilt.

The data corresponding to the CSU-SS are obtained from Fig. 10 while the data obtained with the RSB-SS are obtained from Fig. 11. Each color represents a linear fit of a single B-scan

Optics EXPRESS

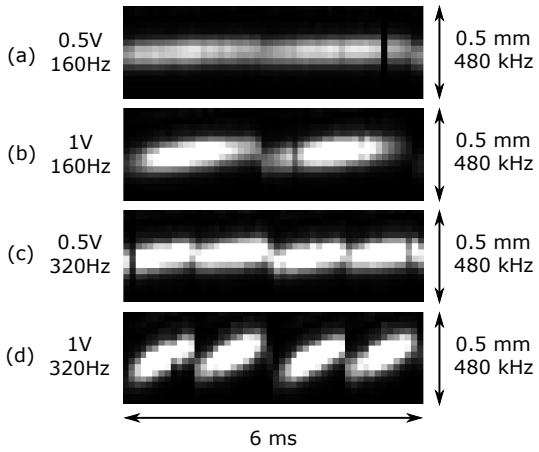

Fig. 11. Comparison of B-scans obtained with the RSB-SS in the configuration (e), only the B-scans from the blue to red (forward) sweep are being presented for different settings of the signal driving the line galvanometer scanner only, considered as GS in Fig. 1. By doubling the frequency of the signal applied to the GS but halving the amplitude, the speed of the galvanometer scanner remains the same, which in theory should lead to the same ADE value. In (a) and (b), the full period of the driving signal is shown, while in (c) and (d), twice that period.

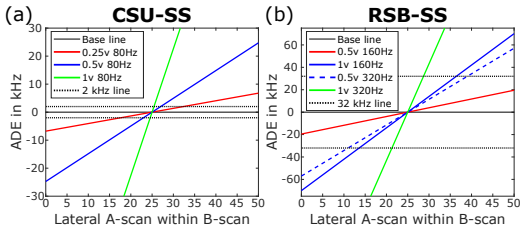

Fig. 12. Tilt of T-scans in the B-scans obtained for different frequency of the signal applied to the GS with the CSU-SS (a) and RSB-SS (b) against the T-scan obtained with the sample beam stationary (base line) calculated in configuration (e). The vertical axis corresponds to the ADE in kHz while the horizontal axis corresponds to the lateral position in the B-scan. The insets show the settings used for the GS driving signal. The horizontal dotted lines correspond to the frequency resolution of the spectrum sampling, as determined by the sweeping frequency of each source, 32 kHz for the RSB-SS and 2 kHz for the CSU-SS. Any value between these dotted lines in each graph would not be lead into visible ADEs in the B-scans.

from each of the settings used for each figure. The base angle deviation of the GS mirror was measured by applying offsets of -0.5 V, 0 V and 0.5 V, to its driver. Finally, the base angle was substracted from the fits to measure strictly the deviation produced by the ADE,leaving the base line constant at 0 (presented in solid blackline in both figures).

These curves are specific for the sweeping rates of the two swept sources employed. By increasing the swept source rate, the interval between the two dashed lines in both figures increases, and correspondingly, the number M of A-scans as a manifestation of better accomplishment of inequality (9).

Optics EXPRESS

5. Prediction of the sweep direction

As seen in previous figures, the Doppler shift adds to or reduces the frequency of the photodetected signal due to the two sweeps, sweep 1 and sweep 2 as labeled in Fig. 4. The ADEs in the two sweeps are of opposite signs. The ADE also changes sign based on the slope of the ramp of the signal applied to the GS, with one ramp experiencing a reduction of the observed OPD and the other an increase. For ease of calculations, the analysis in this section is restricted to the configuration (s), where a constant ADE is present during each half period T.

When the spectral filter in the swept source uses a resonant scanner (RS), the instantaneous sweeping direction during each half period, τ, of the signal applied to the RS, in term of lowering or increasing the wavelength generated, cannot be easily determined, as any optical spectrum analyzer produces a spectrum for an average of sweeps. The RS cannot be tuned to lower frequency rates in order to enable the use of an optical spectrum analyzer. Synchronizing an optical spectrum analyzer at 16 kHz would be difficult. It is demonstrated here that by using a galvanometer scanner in the OCT interface optics and a tilted mirror as an object, by measuring the resulting ADE, the sweeping direction of a swept source can be determined. Differences in the B-scans due to sweeping direction are evident, but from these images the sweeping direction nor the direction of deflection can be estimated. As the combination of f (due to sweeping) with F (Doppler shift) depends on both signs of the lateral scanning and of the sweeping, a simple procedure was developed to identify the direction of lateral scanning in the images produced. To this goal, the measurements described below are presented.

As illustrated in Fig. 13(a), first, one of the edges of the scanned area of the sampled mirror is covered partially using an opaque screen, OS, in order to differentiate between each ramp of the galvoscanner driven, from now on, considered as GS in Fig. 1. If the right side of the object imaged, when the GS scans from left to right is covered, then the part of the image end of the ramp will be black. When the GS scans from right to left, the beginning of the ramp will be missing in the image. In this way some relation can be established between time and lateral position. The swap of scanning direction from left-right to right-left will not be seen, but the transition from right – left to left – right will remain visible, therefore named Visible Transition, VT.

This procedure allows us to quickly determine in a set of consecutive B-scans which B-scan corresponds to which ramp of the triangular driving signal, by simply looking at the transition between B-scans and the location of the black sectors in the images so produced.

In Fig. 13, the effect on the B-scans obtained using the RSB-SS is documented. In (b), a photo of the setup is shown while in (c,d), the B-scans without the opaque screen are (c) while (d) are the B-scans with the opaque screen in place. The VT changes shape between Sweep 1 and Sweep 2, consequence of a different ADE sign for each sweep as shown.

The 4 consecutive B-scans presented in Fig. 13 were obtained at 333 Hz (i.e., 2T = 3 ms). On the top row there are B-scans obtained with sweep 1, while on the bottom there are B-scans obtained with sweep 2. During the VT, those in sweep 1 follow a pattern “down-up” while the others in sweep 2 follow a pattern “up-down”.

In order to determine the sign of the ADE based on the sweeping direction, the RSB-SS was replaced with the CSU-SS, for which the direction of sweeping is known, and the measurements covering the mirror were repeated as performed in the process of obtaining Fig. 13. The Superlum Broadsweeper 840 sweeps from red to blue (backwards), starting at 873 nm and finishing the sweep at 828 nm, at a maximum 2 kHz sweeping rate.

The GS was run with a triangular ramp of 2T = 3 ms. Since the CSU-SS sweeps at a slower rate of ~ 1.8 kHz, instead of the 32 kHz for the RSB-SS, images are generated by compounding up to 20 consecutive B-scans in Fig. 14, to enhance both “down-up” and “up-down” transitions. Each B-scan is composed from a number of A-scans that is obtained by: M = 1.8 kHz/0.66 = 2.7 A-scans per each half period T = 1.5 ms.

Optics EXPRESS

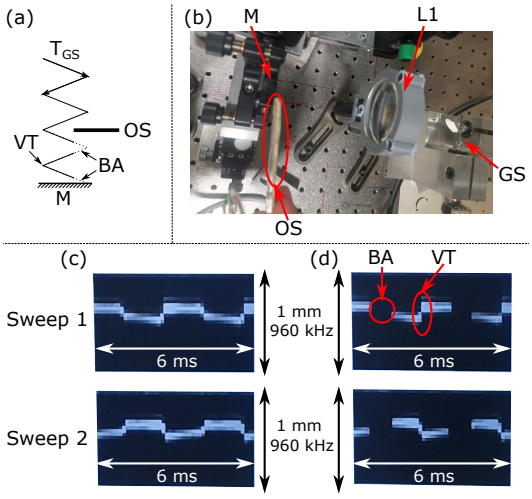

Fig. 13. Procedure to determine the sweep direction. (a) Schematic representation of time associated to a lateral portion of the T-scan in the B-scan. T_{GS}: trajectory of laterally scanned beam by GS in time; An opaque screen (OS) blocks partially the scanned area; BA: black area in the image due to the OS; VT: visible transition. (b) Aerial view of the interface optics showing the galvanometer scanner head (with the frame scanner axis horizontal and fixed and the line scanner vertical, used as GS in Fig. 1, determining horizontal deflections), the lens L1, the mirror M and the OS covering one of the edges of the scanned area; (c) B-scans separated for the two sweeps of the RSB-SS; (d) The same images on the left but displaying the effect of the OS, obscuring the area marked as BA and leaving only a portion of the object as the visible transition, VT, in the B-scan image between the deflection from right to left and deflection from left to right.

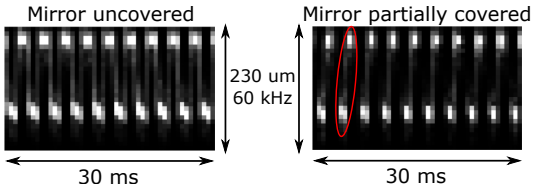

Fig. 14. Results obtained from 20 consecutive B-scans with the CSU-SS at 333 Hz and 0.2 V amplitude. When partially covering the mirror as shown in Fig. 13, CSU-SS replicates the pattern "down-up" marked in red. The measured ADE peak-peak is 32 kHz.

Since the setup can only record full A-scans, 2.7 means that sometimes we will record 2 A-scans per B-scan and sometimes 3, hence we collected 20 B-scans. A video is recorded from which 9 frames of 20 B-scans each are acquired, and averages were produced with them. Otherwise, transitions are not visible in the compounded images due to the slow acquisition speed.

The results are presented in Fig. 14. The B-scans present a peak to peak ADE interval of 122 µm or 32 kHz, i.e., 16 kHz per each sweeping direction. On the left, there are B-scans obtained with the mirror uncovered, and on the right there are B-scans obtained by blocking the right side of the mirror under imaging, same side as in Fig. 13. The transition shown within the window VT, after blocking the mirror with the opaque screen as illustrated in Fig. 13 top is "Down-Up", the same transition as we observed in the sweep 1 in Fig. 13 when using the RSB-SS. We can then infer that on the RSB-SS, the sweep 1 in Fig. 13 corresponds to a sweep from red to

Optics EXPRESS

blue (backward), while the sweep 2 corresponds to blue to red (forward). This represents an interesting application of the current study, an optical spectral characterization made possible by employing an interferometer, a deflector and an opaque screen.

It can be noticed that the ADE is larger on the CSU-SS, which runs at ~ 2 kHz, than for the RSB-SS, running at 32 kHz, but this is expected, as the ratio 2 kHz/666 Hz is 16 times smaller than 32 kHz/666 Hz, in agreement with Eq. (6).

6. ADE validation using a fast swept source

While sources at 850 nm are more limited on their speed, higher sweeping frequencies are achieved at longer wavelengths [14,15]. A valid question would be if ADE is also relevant for swept sources widely used by the OCT community at 1060 and 1300 nm, sweeping at over 100 kHz. Unfortunately, we did not have any bidirectional swept source to perform the study apart from the swept source own assembled at 32 kHz used above, at 850 nm. Hence, in this section we do not intend to reproduce all the steps presented above at 850 nm, but to prove only that axial distortion of B-scan contours still occur at faster sweeping rates.

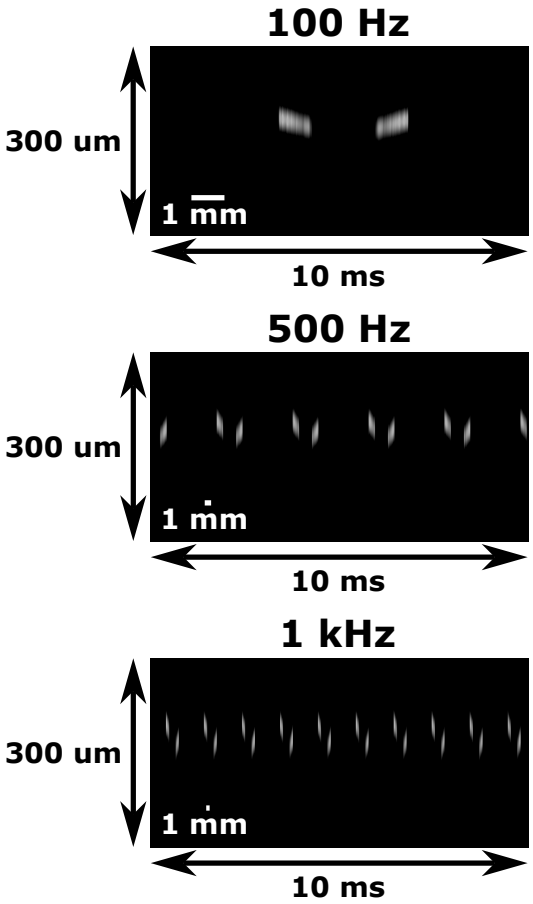

Fig. 15. B-scans obtained from a 1 mm section of a slightly tilted mirror with the CFU-SS Axsun source operating at 1060 nm and 100 kHz sweeping rate. All images are obtained in 10 ms and span 300 μm in depth. From top to bottom, different lateral scanning frequencies, $1/2T$ are presented, with first at 100 Hz, second 500 Hz and third 1 kHz.

Optics EXPRESS

We acquired data in a setup similar to that of Fig. 3, designed for imaging the eye and paired with a commercial fast unidirectional swept source (CFU-SS) from Axsun at 1060 nm sweeping at a 100 kHz sweeping rate. A rigorous study with quantitation of tilt using a broadband source as in previous sections was not possible and therefore simply placing the mirror as a target could not guarantee an exact (s) or (e) configurations due to the large spherical aberrations of the interface optics in such a system. The line (fast) galvanometer scanner, playing the role of GS in Fig. 1 of the setup was driven with a triangular signal at different frequencies, ranging from 100 Hz to 1 kHz. The results are presented in Fig. 15, and were obtained by scanning 2 V amplitude across a slightly tilted mirror from which only 1 mm was exposed by placing a slit in front of the mirror to minimize the effect of the large aperture, creating an approximation of the configuration (s), and presenting pairs of consecutive B-scans corresponding to each slope of the GS. The B-scans in Fig. 15 show a tilt of 80 μm of the mirror measured from one edge to the other of its lateral size.

At 100 Hz no ADE is perceptible, the B-scan image for the other side of the ramp of the triangular signal shows the top of the B-scan at a similar axial position. However, by increasing the lateral scanning frequency, the two contours slips in relation to each other as shown for 500 Hz and 1 kHz. The deviation of contours became apparent at 200 Hz, with minimal deviation, and at 500 Hz where the deviation is better visible. The distance between the two contours corresponding to the two ramps is ~ 13 μm, which implies an ADE of ~ 6.5 μm in each B-scan. The ADE approximately doubles up to ~ 13 μm when doubling the frequency to 1 kHz, leading to a total deviation of ~ 26 μm, that represents ~ $2.9a$, considering the axial resolution a ~ 9 μm. At the top, where no ADE is visible, M = 500, while at the bottom, with M = 50 only, where ADE is clearly manifest.

7. Conclusions

The paper presents a distorting effect of contours in the B-scan OCT images that happens in SS-OCT when the number of sweeps per lateral scanning interval is small and specular layers are tilted in respect to the wavefront established by the scanning beam. Two swept sources at 850 nm were evaluated, one unidirectional at 2 kHz (CSU-SS), the other bidirectional at 32 kHz (RSB-SS), in two configurations, as used for imaging skin or imaging the retina. A third unidirectional fast source at 1060 nm (CFU-SS) at 100 kHz was used in a skin configuration to prove that the ADE may present a problem even when using fast swept sources. With continuous progress in the technology of swept sources, more bidirectional sources will be reported, in which case the error documented here doubles in comparison to that for unidirectional sweeping.

The distortion manifests in displacement of structure in the B-scan along its depth, due to the Doppler shift imprinted by lateral scanning. For each lateral pixel, its depth position is altered axially by an ADE. As long as ADE is less than the axial resolution interval, a, such error is not visible. As a rule of thumb, the ADE affects all systems depending on the threshold of path difference δ due to tilt, established by Eq. (9): when δ/M exceeds $\lambda/2$, where M is the number of lateral pixels, given by the ratio T/τ. The ADE is observable at slow as well as at fast sweeping rates, and the deciding factor is not the sweeping speed, $1/\tau$ but the ratio M. For instance, for the three systems used: in Fig. 6, at 2 kHz, M ~ 13, in Fig. 8, using the 32 kHz bidirectional, M ≃ 48 at 333 Hz, and using the fast source at 100 kHz, in Fig. 15, M = 500, 100 and 50 in the three cases shown, depending on the lateral scanning frequency.

So irrespective of sweeping speed, ADE becomes insignificant if larger M values are used. In general, the OCT community employs large number M of pixels and perhaps this is why such an effect has not been documented so far. There is some fundamental value in Eq. (9), that OCT developers should be aware of, as the number of half wavelengths exceeded by δ/M is equivalent to the number of axial resolution intervals in the ADE.

Optics EXPRESS

The authors are unaware of prior reports documenting such axial errors of contours of specular tilted targets described here, depending on the direction of the lateral scanning, direction of sweeping and object layer tilt.

The ADE demonstrated here have been kept at minimum values by proper adjustment of the interface optics and with due attention given to the beam incident on the two galvanometer scanner, each to be placed on the rotation axis of the respective galvoscanner. However larger deviations were observed for improper adjustment of the interface optics which were not included here. The variations in OPD during scanning can be exacerbated by incorrect lateral adjustment of lens position L1 in Fig. 1(s) or of the telescope of lenses L1 and L2 in Fig. 1(e). As noticed in the TD-OCT practice, more fringe cycles are created in the C-scan time display in Fig. 5 if the incidence of the beam is moved away from the pivot of the GS, or the mirror used as a sample is tilted. Only the simplest cases of a tilted mirror in the (s) configuration and of a horizontally flattened contour of the retina in the (e) configuration have been considered. In practice however, equivalent path deviations, as δ here can be created by off axis placement of lenses or incidence beam not exactly on the rotation pivot of either galvanometer scanner, with the most attention needed to the line scanner, that is driven faster. Therefore it is expected that ADE to be larger than that estimated by the Eq. (9) due to improper adjustment of lateral scanners and interface optics. Similar studies as presented here for the two simplified cases of (s) and (e) in Fig. 1 can be performed by writing explicit dependence of optical path versus deviation angle.

Driven by the need for quantitate the ADE, we have also noticed that ADE generation can find some useful application. In this respect, the paper also shows how the direction of sweeping can be determined without using an optical spectrum analyzer. This is important in determining the sweeping direction when employing resonant scanners, where a spectrum analyzer cannot be used to check the sweeping direction. By observing which transitions in the B-scan due to the ADE are observed depending on the direction of lateral scanning, the direction of sweeping can be predicted. Hence this study shows that a simple method can be devised to establish the tuning laser direction, based on a lateral scanner and an interferometer only.

While the effects described in this paper are not normally encountered in the SS-OCT practice, it is expected that they may be easier observed if more bidirectional sweeping lasers are developed, as the ADE is double to that of unidirectional sweeping sources. As the development of bidirectional lasers progresses, users should be aware of such errors introduced and image distortions, that may prevent accurate measurements of axial position of contours and image presentation of moving targets, such as blood molecules in vessels inspected by OCT Angiography.

Funding. University of Kent (17905304, 206593); Invention for Innovation (NIHR202879); Engineering and Physical Sciences Research Council (EP/X000125/1); H2020 Excellent Science (860807, H2020-EU.1.3.1); National Institute for Health Research Biomedical Research Centre at Moorfields Eye Hospital NHS Foundation Trust and UCL Institute of Ophthalmology (BRC4-05-RB413-302).

Acknowledgments. The authors wish to acknowledge the whole Applied Optics Group for their constant support and aid, specially George Dobre for his support on the bidirectional laser and Adrian Bradu and Manuel Marques for their support with the different vi software developed on LabVIEW. Special thanks must be given to Alejandro Martinez for his quick aid preparing the 1060 setup.

Disclosures. AP and AF are co-inventors on OCT patents in the name of the University of Kent.

Data availability. Data underlying this study are available from the authors upon reasonable request.

References

1. G. Haeusler and M. W. Lindner, ""Coherence radar" and "Spectral radar"- new tools for dermatological diagnosis," J. Biomed. Opt. **3**(1), 21–31 (1998).
2. S. Taplin, A. G. Podoleanu, D. J. Webb, *et al.*, "Displacement sensor using channelled spectrum dispersed on a linear CCD array," Electron. Lett. **29**(10), 896–897 (1993).
3. B. Golubovic, B. E. Bouma, G. J. Tearney, *et al.*, "Optical frequency-domain reflectometry using rapid wavelength tuning of a Cr^{4+}:forsterite laser," Opt. Lett. **22**(22), 1704–1706 (1997).
4. A. G. Podoleanu, G. M. Dobre, and D. A. Jackson, "En-face coherence imaging using galvanometer scanner modulation," Opt. Lett. **23**(3), 147–149 (1998).

Optics EXPRESS

5. A. G. Podoleanu, G. M. Dobre, D. J. Webb, *et al.*, "Coherence imaging by use of a Newton rings sampling function," Opt. Lett. **21**(21), 1789–1791 (1996).
6. L. An and R. K. Wang, "Use of a scanner to modulate spatial interferograms for in vivo full-range Fourier-domain optical coherence tomography," Opt. Lett. **32**(23), 3423–3425 (2007).
7. H. C. Hendargo, R. P. McNabb, A.-H. Dhalla, *et al.*, "Doppler velocity detection limitations in spectrometer-based versus swept-source optical coherence tomography," Biomed. Opt. Express **2**(8), 2175–2188 (2011).
8. A. G. Podoleanu, S. R. Taplin, D. J. Webb, *et al.*, "Theoretical study of talbot-like bands observed using a laser diode below threshold," Pure and Applied Optics: Journal of the European Optical Society Part A **7**(3), 517–536 (1998).
9. W. Drexler, J. G. Fujimoto, and E. Greenbaum, eds., *Optical Coherence Tomography: Technology and Applications*, Biological and Medical Physics, Biomedical Engineering (Springer, Berlin, Heidelberg, 2008).
10. J. P. Fingler, "Motion Contrast Using Optical Coherence Tomography," phd, California Institute of Technology (2007).
11. G. Venugopal, G. Dobre, A. Chamorovskiy, *et al.*, "Development of a 850nm swept source based on a resonant scanner spectral filter," in *Optical Coherence Imaging Techniques and Imaging in Scattering Media V*, vol. 12632 (SPIE, 2023), pp. 222–224.
12. A. G. Podoleanu, "Optical coherence tomography," J. Microsc. **247**(3), 209–219 (2012).
13. L. An, H. M. Subhash, and R. K. Wang, "Full range complex spectral domain optical coherence tomography for volumetric imaging at 47 000 A-scans per second," J. Opt. **12**(8), 084003 (2010).
14. D. Huang, F. Li, C. Shang, *et al.*, "Reconfigurable time-stretched swept laser source with up to 100 mhz sweep rate, 100 nm bandwidth, and 100 mm oct imaging range," Photon. Res. **8**(8), 1360–1367 (2020).
15. T. Pfeiffer, M. Petermann, W. Draxinger, *et al.*, "Ultra low noise fourier domain mode locked laser for high quality megahertz optical coherence tomography," Biomed. Opt. Express **9**(9), 4130–4148 (2018).